Available online at www.sciencedirect.com

ScienceDirect

Procedia Engineering 148 (2016) 646 – 653

Procedia Engineering

www.elsevier.com/locate/procedia

4th International Conference on Process Engineering and Advanced Materials

Promotional Effect of Ce-dopant on Al_2O_3-supported Co Catalysts for Syngas Production via CO_2 Reforming of Ethanol

Fahim Fayaz[a], Huong T. Danh[b], Chinh Nguyen-Huy[c], Khanh B. Vu[d], Bawadi Abdullah[e], Dai-Viet N. Vo[a,f,*]

[a]*Faculty of Chemical & Natural Resources Engineering, Universiti Malaysia Pahang, Lebuhraya Tun Razak, 26300 Gambang, Kuantan, Pahang, Malaysia*
[b]*Clean Energy and Chemical Engineering, Korea University of Science and Technology (UST), Deajeon, 305-350, Korea*
[c]*School of Energy & Chemical Engineering, UNIST, 50 UNIST-gil, Eonyang-eup, Ulju-gun, Ulsan 689-798, Republic of Korea*
[d]*NTT Hi-Tech Institute, Nguyen Tat Thanh University, 298-300A Nguyen Tat Thanh Street, Ho Chi Minh City, Vietnam*
[e]*Chemical Engineering Department, Universiti Teknologi PETRONAS, 32610 Seri Iskandar, Perak, Malaysia*
[f]*Centre of Excellence for Advanced Research in Fluid Flow, Universiti Malaysia Pahang, 26300 Gambang, Kuantan, Pahang, Malaysia*

Abstract

The effect of ceria promotion on Co/Al_2O_3 catalysts for ethanol dry reforming has been investigated at stoichiometric feed composition and 973 K under atmospheric pressure. Ce-promoted catalysts were synthesized using a wet co-impregnation method and evaluated in a quartz fixed-bed reactor. X-ray diffraction measurements indicated the formation of CeO_2, Co_3O_4 and $CoAl_2O_4$ phases on catalyst surface. Ce-addition eased the reduction process of Co_3O_4 to CoO phase which was subsequently reduced to metallic Co^0 form. H_2 and CO yields as well as ethanol conversion increased with growing Ce loading and approached the greatest value at 3wt.%Ce followed by a considerable drop beyond this optimal Ce content. Both promoted and unpromoted catalysts were stable with time-on-stream and the improvement of catalytic performance with Ce-addition was reasonably due to the high oxygen storage capacity of CeO_2 promoter which oxidizing carbonaceous species. The heterogeneous nature of deposited carbons containing carbon nanofilament and graphite on spent catalyst surface was evident by scanning electron microscopy. However, the filamentous carbon appeared to be predominant on the surface of spent catalyst in comparison with undesirable graphite responsible for catalyst deterioration. Additionally, Ce-promoted catalysts were resistant to carbon deposition.

Peer-review under responsibility of the organizing committee of ICPEAM 2016

Keywords: Co-based catalysts; Ethanol CO_2 reforming; Ethanol dry reforming; Hydrogen; Syngas

* Corresponding author. Tel.: +6-095-492-874; fax: +6-095-492-889.
E-mail address: vietvo@ump.edu.my

Peer-review under responsibility of the organizing committee of ICPEAM 2016
doi:10.1016/j.proeng.2016.06.530

1. Introduction

The increasing anthropogenic greenhouse gas emissions owing to the excessive combustion of fossil fuels for globally economic development have resulted in a significantly negative impact on the environment including global warming and climate change. A renewable and green energy is required urgently for replacing petroleum-based resources in order to reduce the substantial dependency on crude oil and its undesirable influence on atmosphere. Syngas, a mixture of H_2 and CO has been considered as a potential and promising sustainable energy from an economic and environmental point of view [1]. Conventionally, syngas can be generated from several common approaches, namely, methane steam or dry reforming [2,3] and partial oxidation [4,5].

However, there have been considerably renewed interests on ethanol dry reforming, EDR (cf. Eq. (1)) for syngas production since this process not only generates a syngas with preferred H_2/CO ratio for downstream methanol and long-chain hydrocarbon synthesis [6,7] but also captures CO_2, a greenhouse gas to form value-added products. In addition, among renewable reactants, ethanol has been viewed as an alluring H-containing feedstock due to its high availability, low toxicity and ease of handling [8,9].

$$C_2H_5OH + CO_2 \rightarrow 3H_2 + 3CO \ (\Delta H^0_{298K} = 296.8\,\mathrm{kJ\,mol^{-1}}) \quad (1)$$

Ni-based catalysts are widely used for EDR reaction due to their outstanding ability of breaking the C-C bond of ethanol [6,10]. Zawadzki *et al*. studied the effect of support type on the performance of EDR and found that CeO_2-supported Ni catalyst exhibited high C_2H_5OH conversion, X_{C2H5OH} and resisted to coke deposition because of the facile reduction process and the redox properties of CeO_2 [6]. Bellido *et al*. reported that 5%Ni/Y_2O_3-ZrO_2 catalyst possessed an optimum X_{C2H5OH} of about 61% at 1073 K [11]. However, Ni-based catalyst reportedly suffered from the formation of carbonaceous deposition [6,10,11]. Raman analysis of spent Ni catalysts after EDR identified co-existence of filamentous and graphitic carbons produced from Boudouard reaction (Eq. (2)), methane decomposition (Eq. (3)) and ethylene polymerization (Eq. (4)) [6,12].

$$2CO \rightarrow C + CO_2 \ (\Delta H^0_{298K} = -172.4\ \mathrm{kJ\,mol^{-1}}) \quad (2)$$

$$CH_4 \rightarrow C + 2H_2 \ (\Delta H^0_{298K} = 75.0\,\mathrm{kJ\,mol^{-1}}) \quad (3)$$

$$C_2H_5OH \rightarrow C_2H_4 \rightarrow polymerization \rightarrow \mathrm{Coke} \quad (4)$$

Supported Co catalysts are also the common catalysts for syngas production from dry reforming of methane [13,14] and ethanol steam reforming [15,16] owing to their affordable cost, high activity and stability. However, to the best of our knowledge, there were limited or no studies about Co catalyst and the promotional effect of rare-earth metal oxides on its catalytic properties and activity for EDR reaction. Thus, this paper aimed to investigate the influence of Ce promoter on the physicochemical attributes and performance of Al_2O_3-supported Co catalysts for EDR reaction.

2. Experimental

2.1. Catalyst synthesis

Wet co-impregnation method was employed for synthesizing X%Ce-10%Co/Al_2O_3 catalysts with X being 0-5%wt. An accurately balanced amount of $Ce(NO_3)_3.6H_2O$ and $Co(NO_3)_2.6H_2O$ aqueous solutions (supplied by Sigma-Aldrich) was mixed with γ-Al_2O_3 support (Puralox SCCa-150/200 from Sasol) previously calcined in air at 1023 K for 5 h with a heating rate of 5 K min^{-1} to guarantee thermal stability. The slurry mixture was magnetically stirred for 3 h at room temperature and subsequently dried at 383 K overnight. The dried solid was further air-

calcined at 773 K for 3 h to obtain X%Ce-10%Co/Al_2O_3 catalysts. Catalyst was crushed and sieved to an average particle size of 125-160 μm before being subjected to EDR evaluation.

2.2. Catalyst characterization

The crystal structure of both unpromoted and Ce-promoted 10%Co/Al_2O_3 catalysts was examined in a Rigaku Miniflex II X-ray powder diffraction system. Cu target was employed as radiation source with wavelength, λ of 1.5418 Å and operated at 30 kV and 15 mA. The diffraction patterns were recorded from 2θ = 3° to 80° with small scan speed and step size of 1° min^{-1} and 0.02° in that order to capture a high resolution. A Micromeritics AutoChem II-2920 chemisorption system was employed for conducting H_2 temperature-programmed reduction (H_2-TPR). Approximately, 0.1 g of catalyst was placed in a quartz U-tube and sandwiched by quartz wool. After a pretreatment at 373 K for 30 min in flowing He gas of 50 ml min^{-1}, specimen was heated with a linear rate of 10 K min^{-1} from 373 to 1173 K under 50 ml min^{-1} flow of 10%H_2/Ar and held at this temperature for 30 min.

Scanning electron microscopy (SEM) images of fresh and spent X%Ce-10%Co/Al_2O_3 catalysts were also performed on a Carl Zeiss AG-EVO® 50 series apparatus using a SmartSEM software to examine the morphological surface and type of carbonaceous deposition. Additionally, in order to quantify the amount of deposited carbon on catalyst surface after EDR reaction, temperature-programmed oxidation (TPO) runs were performed for used catalysts on a TGA Q500 unit (TA Instruments). Spent catalyst was initially preheated at 373 K with a temperature ramp of 10 K min^{-1} for 30 min in 100 ml min^{-1} of N_2 for assuring the complete removal of moisture and associated volatile compounds. It was then subjected to oxidation in a mixture of $4N_2$:$1O_2$ (100 ml min^{-1}) from 373 to 1023 K at a heating rate of 10 K min^{-1}. Specimen was further kept isothermally at this temperature for 30 min before being cooled down to room temperature in the similar gas mixture.

2.3. Ethanol dry reforming experiment

Ethanol dry reforming runs were carried out in a quartz fixed-bed reactor (L = 17 inches and O.D. = 3/8 inches) placed vertically in a split tubular furnace at a stoichiometric CO_2:C_2H_5OH ratio of 1:1 and reaction temperature of 973 K under atmospheric pressure. Both gaseous reactant, CO_2 and N_2 diluent were accurately regulated by electronic Alicat mass flow controllers whilst ethanol was precisely pumped into the reactor using a syringe pump (KellyMed KL-602). The partial pressure of CO_2 and C_2H_5OH was kept at 20 kPa during reaction and N_2 inert gas was employed as a tie-component for material balance purposes and ensuring the total inlet flow rate of 70 ml min^{-1}. Approximately, 0.1 g_{cat} of catalyst was mounted by quartz wool in the middle of reactor and high gas hourly space velocity (GHSV) of 42 L g_{cat}^{-1} h^{-1} was used for all runs to guarantee the negligible internal and external transport intrusions under the reaction conditions. The composition of gaseous effluent from the outlet of reactor was analyzed on an Agilent GC 6890 series gas chromatograph using thermal conductivity detector (TCD) and flame ionization (FID) detectors.

3. Results and Discussion

3.1. X-ray diffraction measurements

The XRD patterns of calcined γ-Al_2O_3 support, unpromoted and Ce-promoted 10%Co/Al_2O_3 catalysts are shown in Fig. 1. The Joint Committee on Powder Diffraction Standards (JCPDS) database was used to interpret the crystal structure of all catalysts [17]. X-ray diffraction of support was also conducted to use as a reference for comparing with Al_2O_3-supported Ni catalysts. As seen in Fig. 1, gamma-Al_2O_3 phase was detected with typical peaks at 2θ of 32.8º, 37.0º, 44.5º, 45.6º, 56.3º and 67.1º for all catalysts and support. Both Co_3O_4 (2θ of 31.2º and 37.0º) and spinel $CoAl_2O_4$ (with 2θ of 59.4º and 65.3º) phases were identified on the surface of promoted and unpromoted catalysts. The presence of spinel $CoAl_2O_4$ phase would indicate the strong interaction between Co metal oxide and Al_2O_3 support. The peak detected at 2θ = 28.5º belonged to CeO_2 phase for all Ce-promoted catalysts and the increase in intensity of this characteristic peak with growing Ce-loading (cf. Fig. 1(c)-(f)) is symptomatic of the enhancement of

CeO_2 crystallinity. In addition, the appearance of Co_3O_4 and CeO_2 forms was due to the subsequent oxidation of the corresponding CoO and Ce_2O_3 phases formed from the decomposition of $Co(NO_3)_2$ and $Ce(NO_3)_3$ metal precursors, respectively to metal oxides and N_2O_5 gas during air-calcination.

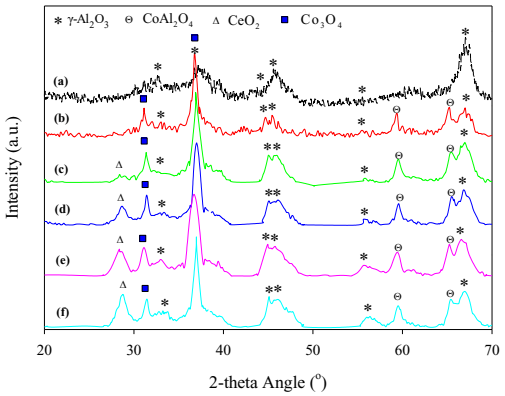

Fig. 1. XRD patterns of (a) calcined γ-Al_2O_3 support, (b) 10%Co/Al_2O_3, (c) 2%Ce-10%Co/Al_2O_3, (d) 3%Ce-10%Co/Al_2O_3, (e) 4%Ce-10%Co/Al_2O_3 and (f) 5%Ce-10%Co/Al_2O_3 catalysts.

3.2. H_2 temperature-programmed reduction

The reducibility of catalysts was studied by H_2-TPR measurements and the H_2-TPR profiles of unpromoted and Ce-promoted 10%Co/Al_2O_3 catalysts are displayed in Fig. 2. There were no detectable reduction peaks observed from TCD signal of γ-Al_2O_3 support (cf. Fig. 2(f)). Thus, any detected peaks of catalysts would belong to the intrinsic reduction property of active metal oxides. It is widely reported in literature that the reduction of Co_3O_4 phase in H_2 is a two-step process via $Co_3O_4 \rightarrow CoO \rightarrow Co^0$ [16,18]. Hence, the low temperature peak, P1 located at 594-709 K was assigned to the formation of CoO phase from Co_3O_4 reduction whilst the second peak, P2 corresponded to the following reduction of CoO intermediate phase to the metallic Co^0 form. The shoulder (P3) at higher temperature of 870-975 K was attributed to the reduction of $CoAl_2O_4 \rightarrow Co^0$ phase [18]. Interestingly, the first peak, P1 was shifted to a lower reaction region for Ce-promoted catalysts indicating the facile reduction of $Co_3O_4 \rightarrow CoO$ with Ce-promotion reasonably due to the increasing electron density donated from CeO_2 promoter easing the reduction process.

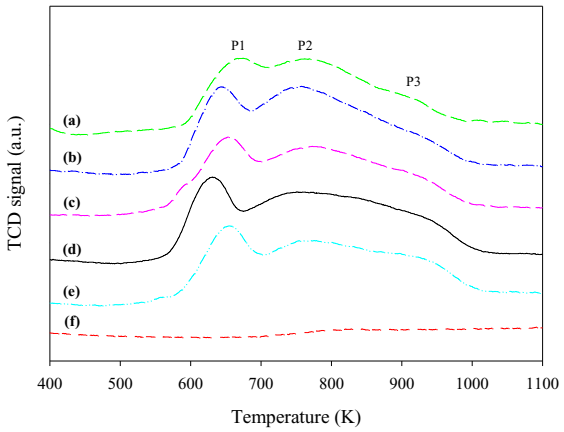

Fig. 2. H_2-TPR profiles of (a) 10%Co/Al_2O_3, (b) 2%Ce-10%Co/Al_2O_3, (c) 3%Ce-10%Co/Al_2O_3, (d) 4%Ce-10%Co/Al_2O_3, (e) 5%Ce-10%Co/Al_2O_3 catalysts and (f) calcined γ-Al_2O_3 support.

3.3. Ethanol dry reforming evaluation

The influence of Ce-promoter loading on C_2H_5OH conversion with time-on-stream (TOS) at stoichiometric feed ratio is shown in Fig. 3. In general, both promoted and unpromoted catalysts exhibited an initially slight drop within 4 on-stream. However, catalytic activity seems to be negligibly changed beyond 4 h. Regardless of Ce loading, promoted catalyst performed greater X_{C2H5OH} than that of the unpromoted counterpart. The enhancement of catalytic activity with Ce-addition was rationally due to the basic property of CeO_2 promoter increasing CO_2 adsorption and its high oxygen mobility establishing a dynamic equilibrium between carbonaceous deposition and coke gasification on catalyst surface [19]. The maximum C_2H_5OH conversion of about 52% was observed at 3wt.%Ce loading. The improvement of X_{C2H5OH} with Ce content was rationally because of increasing basic site concentration with Ce-addition. However, a considerable drop in X_{C2H5OH} was evident for greater Ce loading than 3wt.% reasonably due to the poor dispersion of Co particles and the agglomeration of CeO_2 promoter at high metal loading.

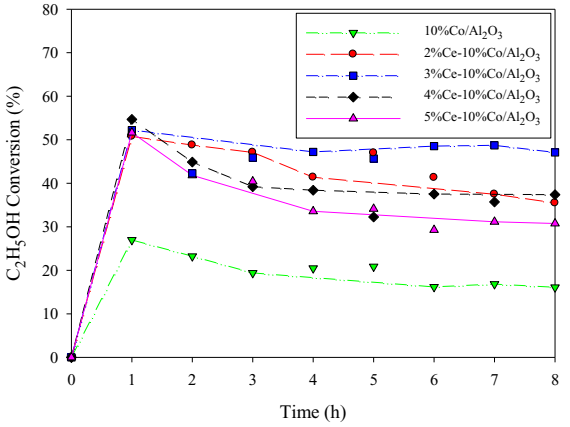

Fig. 3. Effect of Ce loading on C_2H_5OH conversion with time-on-stream at $P_{CO2} = P_{C2H5OH} = 20$ kPa and T = 973 K.

The effect of promoter loading on the yield of products for promoted and unpromoted catalysts is shown in Fig. 4. Interestingly, 3wt.%Ce content was also the optimal loading in terms of H_2 and CO yields whilst CH_4 yield declined with dopant addition and reached to the lowest value of about 6.22% at the same Ce composition. This behavior would suggest the rising secondary reaction, i.e., CH_4 dry reforming converting CH_4 intermediate by-product to H_2 and CO [10]. Thus, the relationship between CH_4 yield and Ce loading experienced a reverse trend as compared to that of H_2 and CO yields *vs.* dopant content (cf. Fig. 4).

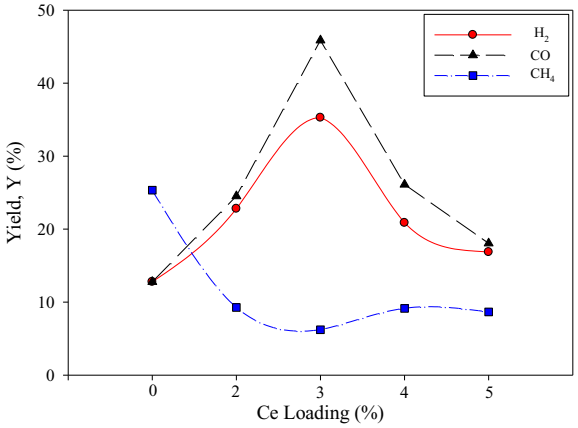

Fig. 4. Influence of Ce content on gaseous product yield at $P_{CO2} = P_{C2H5OH} = 20$ kPa and T = 973 K.

3.4. Postreaction characterization

In order to investigate the surface morphology of fresh catalyst and character of carbonaceous deposits on spent catalyst surface, SEM measurements of selected fresh and spent promoted catalysts were carried out as seen in Fig. 5. The SEM micrograph of fresh 3%Ce-10%Co/Al_2O_3 catalyst (cf. Fig. 5(a)) shows the presence of irregular Co_3O_4 clusters and these crumb-like Co_3O_4 particles reside on the smooth surface of Al_2O_3 support. As seen in Fig. 5(b), it is evident that both carbon nanofilament, CNF (blue rectangle) and graphitic carbon (red round) were formed on catalyst surface during EDR reaction in agreement with other studies [6,12]. Zawadzki *et al.* also reported that graphite and amorphous carbon were formed from the corresponding methane decomposition (cf. Eq. (3)) and polymerization of ethylene (cf. Eq. (4)) reactions [6]. As seen in Fig. 5(b), the amount of CNF, however, seemed to be superior to the quantity of graphite, which may block the access of active metallic surface resulting in catalyst deactivation. These carbonaceous species encircled the surface of catalyst but catalyst was not deteriorated and stable with time-on-stream (cf. Fig. 3) during EDR since the active metal crystallites were not totally encapsulated by deposited carbon and located at the tip of filamentous carbon [20].

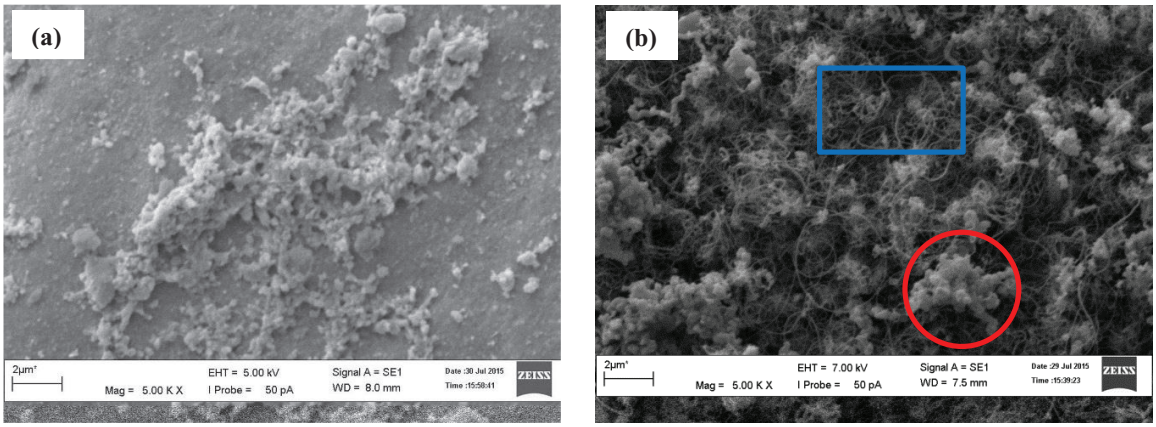

Fig. 5. The SEM microphotographs of (a) fresh 3%Ce-10%Co/Al_2O_3 and (b) spent 3%Ce-10%Co/Al_2O_3 catalysts.

In addition, the percentage of deposited carbon was also quantified by TPO measurements of used catalysts as seen in Fig. 6. Spent unpromoted catalyst possessed the highest carbon content of 51.49% and carbon composition decreased significantly with Ce-addition owing to its high oxygen storage capacity which instantaneously gasifying carbon deposition [19]. Interestingly, 3%Ce-10%Co/Al_2O_3 catalyst was also the optimal catalyst in terms of carbon resilience with 27.94% deposited carbon. As seen in Figs. 3 and 6, the trend of carbon weight vs. Ce loading is opposite to that of X_{C2H5OH} against Ce content further confirming that Ce promotion improved catalytic activity via the oxidization of carbonaceous deposition.

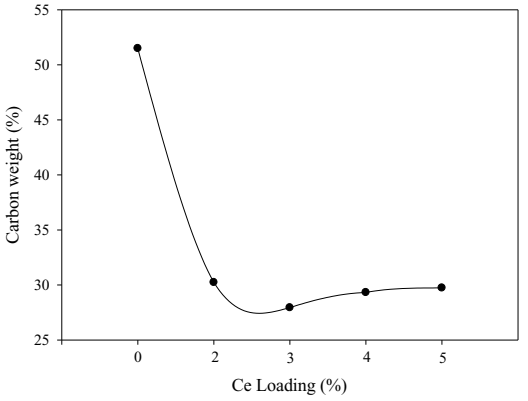

Fig. 6. Effect of Ce loading on carbon content of spent 10%Co/Al_2O_3 catalysts after EDR at P_{CO2} = P_{C2H5OH} = 20 kPa and T = 973 K.

4. Conclusion

Ce-promoted 10%Co/Al_2O_3 catalysts with different Ce loadings have been prepared by a wet co-impregnation method and evaluated for EDR reaction in a quartz fixed-bed reactor at P_{CO2} = P_{C2H5OH} = 20 kPa and 973 K. The appearance of CeO_2, Co_3O_4 and $CoAl_2O_4$ phases on catalyst surface was detected by XRD measurements. H_2-TPR indicated that Co_3O_4 reduction was a two-step process via the formation of a CoO intermediate phase, which was further reduced to metallic Co^0 form. The reduction of Co_3O_4 to CoO phase was facilitated by CeO_2 addition. Both promoted and unpromoted catalysts seemed to be stable with TOS beyond 4 h on-stream and 3wt.%Ce loading was the optimum Ce content in terms of C_2H_5OH conversion, H_2 and CO yields due to the excellent oxygen storage and release ability of CeO_2 promoter. Although filamentous and graphitic carbons were formed on catalyst surface by the corresponding methane decomposition and ethylene polymerization, the surface of catalyst was mainly surrounded by carbon nanofilament.

Acknowledgements

The authors are thankful for the financial support from UMP Research Grant Scheme (RDU130376) to conduct this study. Fahim Fayaz is also grateful for the Graduate Research Scheme Award (GRS) from Universiti Malaysia Pahang (UMP).

References

[1] A. Arslan, S. Gunduz, T. Dogu, Steam reforming of ethanol with zirconia incorporated mesoporous silicate supported catalysts, Int. J. Hydrogen Energy 39 (2014) 18264–18272.
[2] V. Arcotumapathy, F.S. Alenazey, R.L. Al-Otaibi, D.-V.N. Vo, F.M. Alotaibi, A.A. Adesina, Mechanistic investigation of methane steam reforming over Ce-promoted Ni/SBA-15 catalyst, Appl. Petrochem. Res. 5 (2015) 393–404.
[3] S. Zhang, S. Muratsugu, N. Ishiguro M. Tada, Ceria-doped Ni/SBA-16 catalysts for dry reforming of methane, ACS Catal. 3 (2013) 1855–1864.
[4] P. Palacios, M. Toledo, M. Cabrera, Iron ore reduction by methane partial oxidation in a porous media, Int. J. Hydrogen Energy 40 (2015) 9621-9633.
[5] G. Karoshi, P. Kolar, S.B. Shah, G. Gilleskie, L. Das, Calcined eggshell as an inexpensive catalyst for partial oxidation of methane, J. Taiwan Inst. Chem. Eng. 57 (2015) 123-128.
[6] A. Zawadzki, J.D.A. Bellido, A.F. Lucredio, E. M. Assaf, Dry reforming of ethanol over supported Ni catalysts prepared by impregnation with methanolic solution, Fuel Process. Technol. 128 (2014) 432-440.
[7] D.-V.N. Vo, V. Arcotumapathy, B. Abdullah, A.A. Adesina, Non-linear ASF product distribution over alkaline-earth promoted molybdenum carbide catalysts for hydrocarbon synthesis, Catal. Today 214 (2013) 42-49.
[8] A.N. Fatsikostas, D.I. Kondarides, X.E. Verykios, Production of hydrogen for fuel cells by reformation of biomass-derived ethanol, Catal. Today 75 (2002) 145–155.

[9] Ni. Meng, D.Y.C. Leung, M.K.H. Leung, A review on reforming bio-ethanol for hydrogen production, Int. J. Hydrogen Energy 32 (2007) 3238–3247.
[10] X. Hu, G. Lu, Syngas production by CO_2 reforming of ethanol over Ni/Al_2O_3 catalyst, Catal. Commun. 10 (2009) 1633-1637.
[11] J.D.A. Bellido, E.Y. Tanabe, E.M. Assaf, Carbon dioxide reforming of ethanol over Ni/Y_2O_3-ZrO_2 catalysts, Appl. Catal. B: Environ. 90 (2009) 485-488.
[12] A.M. da Silva, K.R. de Souza, G. Jacobs, U.M. Graham, B.H. Davis, L.V. Mattos, F.B. Noronha, Steam and CO2 reforming of ethanol over Rh/CeO2 catalyst, Appl. Catal. B: Environ. 102 (2011) 94-109.
[13] S.Y. Foo, C.K. Cheng, T.-H. Nguyen, A.A. Adesina, Evaluation of lanthanide-group promoters on Co–Ni/Al2O3 catalysts for CH4 dry reforming, J. Mol. Catal. A: Chem. 344 (2011) 28-36.
[14] H. Ay, D. Üner, Dry reforming of methane over CeO2 supported Ni, Co and Ni–Co catalysts, Appl. Catal. B: Environ. 179 (2015) 128-138.
[15] J. Sun, A.M. Karim, D. Mei, M. Engelhard, X. Bao, Y. Wang, New insights into reaction mechanisms of ethanol steam reforming on Co-ZrO2, Appl. Catal. B: Environ. 162 (2015) 141-148.
[16] S. Ogo, T. Shimizu, Y. Nakazawa, K. Mukawa, Steam reforming of ethanol over K promoted Co catalyst, Appl. Catal. A: Gen. 495 (2015) 30-38.
[17] JCPDS Powder Diffraction File, International Centre for Diffraction Data, Swarthmore, PA, 2000.
[18] J.L. Ewbank, L. Kovarik, C.C. Kenvin, C. Sievers, Effect of preparation methods on the performance of Co/Al2O3 catalysts for dry reforming of methane, Green Chem. 16 (2014) 885–896.
[19] T. Hou, S. Zhang, Y. Chen, D. Wang, W. Cai, Hydrogen production from ethanol reforming: Catalysts and reaction mechanism, Renew. Sustain. Energy Rev. 44 (2015) 132-148.
[20] K. de Oliveira-Vigier, N. Abatzoglou, F. Gitzhofer, Dry reforming of ethanol in the presence of A 316 stainless steel catalyst, Can. J. Chem. Eng. 83 (2005) 978-984.